



**HAL**  
open science

# Crystal structure change in magnetocaloric compounds (Er,Nd)<sub>2</sub>Fe<sub>1-7</sub>

Soumaya Louhichi, H. Jaballah, Lotfi Bessais, M. Jemmali

► **To cite this version:**

Soumaya Louhichi, H. Jaballah, Lotfi Bessais, M. Jemmali. Crystal structure change in magnetocaloric compounds (Er,Nd)<sub>2</sub>Fe<sub>1-7</sub>. *Inorganic Chemistry Communications*, 2024, 160, pp.111915. 10.1016/j.inoche.2023.111915 . hal-04377392

**HAL Id: hal-04377392**

**<https://hal.science/hal-04377392>**

Submitted on 2 May 2024

**HAL** is a multi-disciplinary open access archive for the deposit and dissemination of scientific research documents, whether they are published or not. The documents may come from teaching and research institutions in France or abroad, or from public or private research centers.

L'archive ouverte pluridisciplinaire **HAL**, est destinée au dépôt et à la diffusion de documents scientifiques de niveau recherche, publiés ou non, émanant des établissements d'enseignement et de recherche français ou étrangers, des laboratoires publics ou privés.

# Crystal structure change in magnetocaloric compounds $(\text{Er,Nd})_2\text{Fe}_{17}$

S. Louhichi,<sup>1,2</sup> H. Jaballah,<sup>1</sup> L. Bessais,<sup>1</sup> and M. Jemmali<sup>2,3</sup>

<sup>1</sup>Univ Paris Est Creteil, CNRS, ICMPE, UMR 7182, 2 rue Henri Dunant, F-94320 Thiais, France  
<sup>2</sup>University of Sfax, Faculty of Sciences, LSME, BP1171, Sfax 3018, Tunisia.

<sup>3</sup>Department of Chemistry, College of Science and Arts At Ar-Rass, Qassim University, Saudi Arabia  
(Dated: May 1, 2024)

Numerous research studies have documented materials exhibiting a significant magnetocaloric effect (*MCE*) at elevated temperatures. However, there is a scarcity of materials displaying both intriguing *MCE* and a second-order transition phase from a ferromagnetic state to a paramagnetic state at approximately 300 K. In this current study, we provide an account of the structural, magnetic, and magnetocaloric characteristics of the  $(\text{Er,Nd})_2\text{Fe}_{17}$  system.  $(\text{Er,Nd})_2\text{Fe}_{17}$  compound was prepared by arc melting under high pure argon and homogenized at 1073 K to minimize the amount of other possible impurity phases. X-ray diffraction (XRD) coupled with Rietveld analysis with FullProf computer code was used for the structural study. This compound crystallizes in the rhombohedral  $\text{Th}_2\text{Zn}_{17}$  and  $\text{Th}_2\text{Ni}_{17}$  type structure. The  $\text{Er}_{2-x}\text{Nd}_x\text{Fe}_{17}$  compounds adopt the hexagonal  $\text{Th}_2\text{Ni}_{17}$ -structure type and extends for  $x=0, 0.4, 0.7$ , while for  $x= 1.75, 1.85$  and  $2$  adopts the rhombohedral  $\text{Th}_2\text{Zn}_{17}$ -structure type. Hence, the temperature dependence of the magnetization is determined. The Curie temperature increases from 294 K to 335 K after the total Er substitution by Nd. The magnetic entropy changes  $\Delta S_M$ , and the relative cooling power and temperature-averaged entropy change (*TEC*) are reported. Based on these results, the compounds under investigation exhibit an intriguing magnetocaloric effect in the vicinity of room temperature.

PACS numbers: 75.50.Bb, 75.50.Tt, 76.80.+y

Keywords: Intermetallic rare-earth transition-metal compounds; X-Ray Diffraction; Crystal structure, Magnetic materials; Magnetocaloric Effect.

## I. INTRODUCTION

Today's cooling physics is mainly based on vapor compression refrigeration invented a hundred years ago. It has played an important role in industry, agriculture, lifestyle, and housing patterns, ... For example, many commercial applications are available today, including domestic refrigerators, industrial freezers, cryogenics, and air conditioning. However, highly advanced vapor compression refrigeration systems are asymptotically approaching their theoretical efficiency limit. In addition, refrigeration is one ( $\sim 15$  percent) of the largest sources of electricity consumption in the world and therefore contributes to global  $\text{CO}_2$  greenhouse gas emissions. In addition, vapor compression refrigerants themselves, such as hydrochlorofluorocarbons (HCFCs), are one of the major sinks for greenhouse gas emissions, with a global warming potential far greater than that of  $\text{CO}_2$ . As a result, there has been a search for an alternative cooling technology that is highly efficient, economical, and environmentally friendly. In this context, solid-state heat transfer materials, which undergo an adiabatic temperature change or isothermal entropy change when an external stimulus is applied or removed, are highly sought after for new refrigeration solutions to replace current vapor cycle cooling technologies. The most important caloric materials are ferro-ordered materials that often exhibit "giant" caloric effects near their ferroic transitions. Depending on the external stimulus, the effects can be called magnetocaloric (magnetic field), electrocaloric (electric field), or electrocaloric (uniaxial stress). All of these caloric effects seem promising as they can of-

fer better energy efficiency with low environmental impact compared to vapor compression refrigeration. Many important breakthroughs in condensed materials physics and materials science have been made to date through a sustained and coordinated effort by the international caloric community. For example, an important discovery of the giant magnetocaloric effect at room temperature was announced by Karl A. Gschneidner, Jr. and Vitalij K. Pecharsky in 1997, which led to an exponential increase in scientific publications. At the same time, a significant motivation for the development of devices aimed at commercial applications. Several magnetocaloric materials have been studied since the discovery of *MCE*, but the most promising materials for magnetic refrigeration at room temperature are  $\text{Gd}_5(\text{Ge,Si})_4$  [1–4],  $\text{La}(\text{Fe,Co,Si})_{13}(\text{H,C})$  [5–10],  $\text{Fe}_2\text{P}$  [11–14], manganites  $\text{R}_{1-x}\text{A}_x\text{MnO}_3$  [15–18] and related alloys and compounds. Gadolinium is the only element having a strong reversible magnetocaloric effect near room temperature. However, its relatively rapid corrosion by oxidation, its high price, and the insufficient global resources do not allow it to compete with conventional refrigeration systems.  $\text{R}_2\text{Fe}_{17}$  intermetallic compound can be considered as a relatively low-cost magnetocaloric material compared to Gd and Gd-based materials. Additionally,  $\text{R}_2(\text{Fe, X})_{17}$  ( $\text{R}=\text{Pr, Sm, Er, Gd, Ce, Nd}$  and  $\text{X} = \text{Ni, Co, Cu, Mn, Al, Si.}$ ) [19–26] compounds have undergone extensive study over the past two decades, all with the overarching goal of improving both the magnitude and temperature range of *MCE*. We focus on iron-rich  $\text{Er}_2\text{Fe}_{17}$  and  $\text{Nd}_2\text{Fe}_{17}$  based compounds, their relatively large magnetic entropy change maximum around room temperature with a large

full width at half-maximum of magnetic entropy change and its reversible magnetocaloric effect make  $\text{Er}_2\text{Fe}_{17}$  and  $\text{Nd}_2\text{Fe}_{17}$  a good competitor for Gd-based magnetic materials. This research work is part of a continuation of the study of the isothermal section of (Er-Nd-Fe) at 1073 K [27]. The  $\text{Er}_{2-x}\text{Nd}_x\text{Fe}_{17}$  solid solution adopts the hexagonal  $\text{Th}_2\text{Ni}_{17}$  structural model and covers the entire composition range from  $x = 0$  to  $x = 1$ . In contrast, the  $\text{Nd}_{2-x}\text{Er}_x\text{Fe}_{17}$  solid solution, characterized by the rhombohedral  $\text{Th}_2\text{Zn}_{17}$  structure, has a narrow solubility range extending from  $x = 0$  to  $x = 0.3$ . In this work, we select compositions within the solubility limit ranges, considering the significance of phase purity in studying the structural, magnetic, and magnetocaloric properties.

## II. EXPERIMENTAL METHODS

$\text{Er}_{2-x}\text{Nd}_x\text{Fe}_{17}$  has been prepared from high pure elements iron(Fe) 99.9%, erbium (Er) 99.98% and Neodymium(Nd) 99.98% by arc-melting technique under a purified argon atmosphere. The elements are placed in a copper crucible cooled by cold water. After ingot formation, the compound is wrapped in tantalum foil and introduced into a silica tube sealed under secondary vacuum  $2 \times 10^{-6}$  bar [28–30]. The ingot has been heat-treated for seven days at 1073 K, and is finally, water quenched [31–33].

Phase analysis has been performed by X-ray powder diffraction (XRD), using D8 Brucker diffractometer with Cu  $K\alpha$  radiation  $\lambda = 1.54178 \text{ \AA}$ . XRD data of the samples have been collected between  $20^\circ$  and  $80^\circ$  at room temperature with 0.015 step width.

XRD diagrams are analyzed with the Rietveld method [34, 35] using the Fullprof program [36, 37]. The peak shape function has been selected as Thompson-Cox-Hastings pseudo-Voigt type [38]. The goodness of fit indicators  $R_B$  and  $\chi^2$  are calculated from the program output to measure the quality of refinement, and they are defined as [36, 37]:

$$R_B = 100 \frac{\sum_K |I_K(O) - I_K(C)|}{\sum_K I_K(O)}$$

and

$$\chi^2 = \frac{\sum_i w_i |y_i(O) - y_i(C)|}{N - P}$$

where  $I_K(O)$  is the observed Bragg intensity and  $I_K(C)$  is the calculated one.  $y_i(O)$  is the intensity observed at the  $i^{\text{th}}$  step in the step scanned powder diffraction pattern,  $y_i(C)$  is that calculated, and  $w_i$  is the weight of the observation.  $N$  is the total number of points used in the refinement and  $P$  is the number of refined parameters.

The refined parameters are unit cell parameters, scale factors  $U, V, W$ , background points, and atomic positions [39–42], the input atomic parameters have been used to determine the structure of our samples are from Ref. [43–45].

Magnetic properties are measured using a magneto/susceptometer Manics DSM8 operating on the same principle as a Faraday-type balance between 300 and 900 K [46]. A Physical Properties Measurement System (PPMS) magnetometer is used for measurements at low temperatures between 200 and 340 K.

## III. RESULTS AND DISCUSSION

### A. Structure analysis

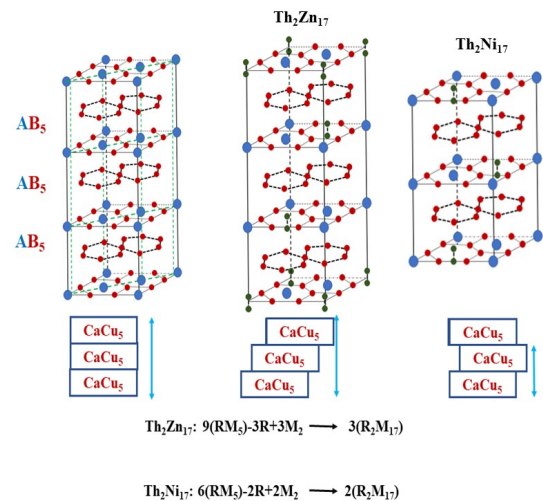


Figure 1.  $P6_3/mmm$  space group with  $\text{Th}_2\text{Ni}_{17}$  type structure et  $R\bar{3}m$  space group  $\text{Th}_2\text{Zn}_{17}$  type structure

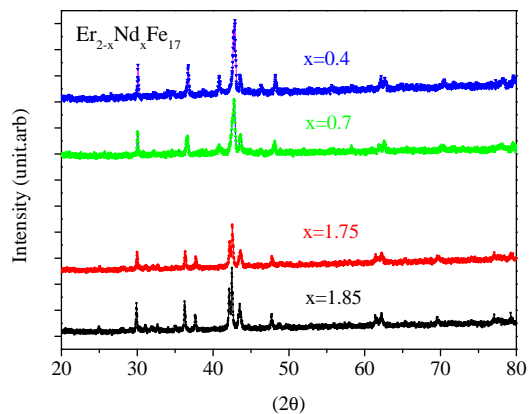


Figure 2. XRD patterns of the  $\text{Er}_{2-x}\text{Nd}_x\text{Fe}_{17}$  ( $x=0.4, 0.7, 1.75$  and  $1.85$ ) samples.

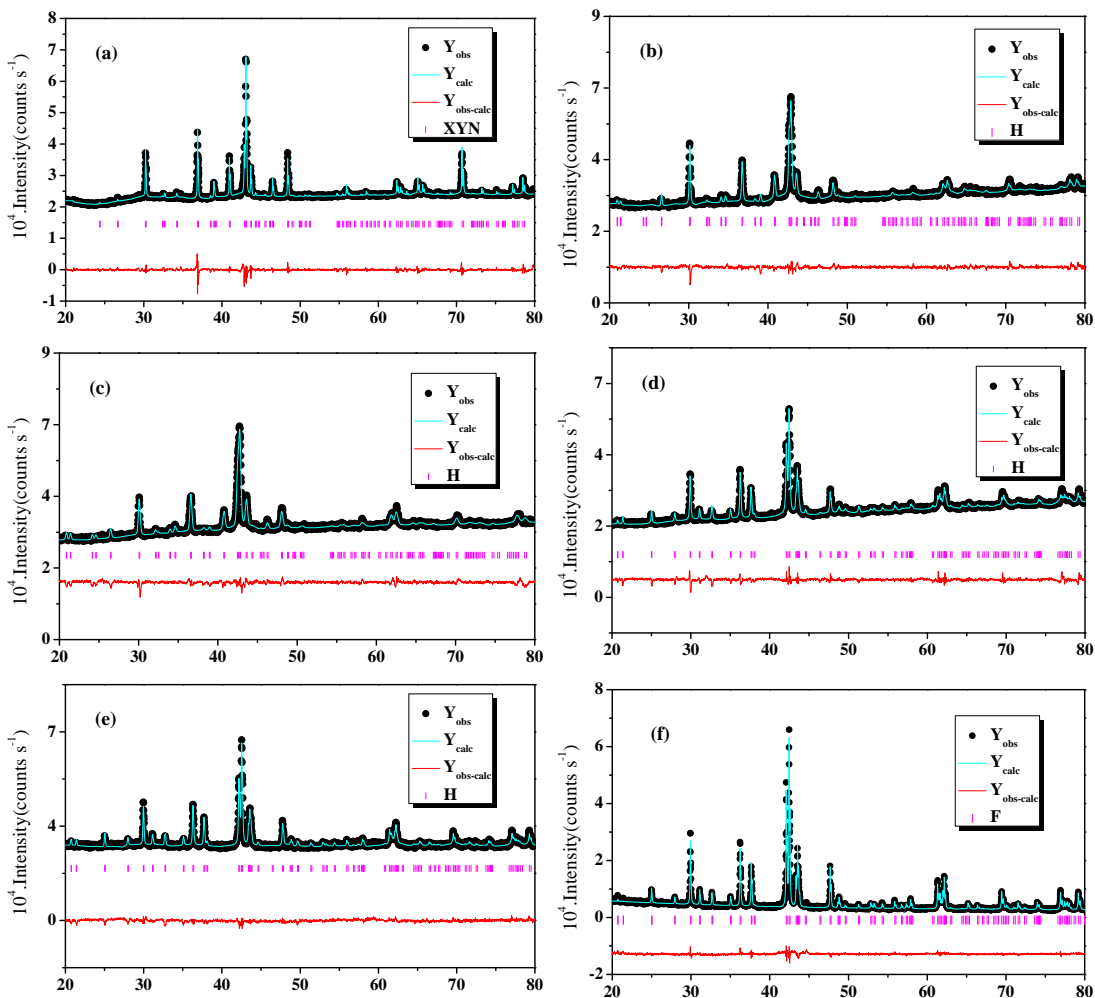


Figure 3. The Rietveld refinement pattern for  $\text{Er}_{2-x}\text{Nd}_x\text{Fe}_{17}$  compounds with  $x=0$  (a),  $x=0.4$  (b),  $x=0.6$  (c),  $1.75$  (d),  $x=1.85$  (e) and  $x=2$  (f). The black circle and cyan lines present respectively the calculated intensities and the experimental intensities. The magenta vertical bars correspond to  $(hkl)$  line positions (Positions of Bragg peaks). The red line shows the difference between the calculated and experimental intensities.

Table I.  $a$  and  $c$  unit cell parameters,  $R_B$ ,  $\chi^2$  factors, and atomic positions from Rietveld refinement of  $\text{Er}_{2-x}\text{Nd}_x\text{Fe}_{17}$ .

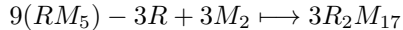
	$x = 0$	$x = 0.4$	$x = 0.7$	$x = 1.75$	$x = 1.85$	2
$a$ (Å)	8.415(3)	8.472(2)	8.507(4)	8.567(1)	8.577(3)	8.581(1)
$c$ (Å)	8.299(4)	8.301(1)	8.308(3)	12.451(1)	12.472(2)	12.491(1)
$c/a$	0.98	0.97	0.97	1.453	1.454	1.455
$V$ (Å <sup>3</sup> )	509	516	521	791	794.57	796
$\chi^2$	1.45	2.28	1.98	2.15	2.44	1.75
$R_B$	2.98	4.13	3.38	3.54	3.75	2.68

Based on their powder diffraction patterns,  $\text{R}_2\text{Fe}_{17}$  compounds are generally assumed to crystallize in the rhombohedral crystal structure of the type  $\text{Th}_2\text{Zn}_{17}$  when  $\text{R}=\text{Pr}$ ,  $\text{Nd}$ ,  $\text{Sm}$  or in the hexagonal structure of the type  $\text{Th}_2\text{Ni}_{17}$  for  $\text{R}=\text{Gd}$ ,  $\text{Tb}$ ,  $\text{Dy}$ ,  $\text{Ho}$ ,  $\text{Er}$ ,  $\text{Tm}$ ,  $\text{Lu}$ . These two structures can be described by a stacking of the  $\text{RM}_5$  ( $\text{CaCu}_5$ ) hexagonal lattice with an ordered re-

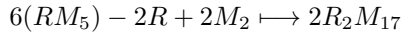
placement of one third of the R atoms by the remaining stoichiometric amount of  $\text{M}_2$  metal pairs:

- The  $\text{Th}_2\text{Zn}_{17}$  type compound has nine entities per cell where three rare earth atoms have each been replaced by a M-M dumbbell (Dumbbell site). This

description can be schematized by:



- $\text{Th}_2\text{Ni}_{17}$  has six entities per unit cell where two rare-earth atoms have been replaced each by a M-M barbell (Dumbbell site). This description can be schematized by :



The rhombohedral structure  $\text{Th}_2\text{Zn}_{17}$  belongs to the  $R\bar{3}m$  space group, where a single  $6c$  site and four different sites  $6c$ ,  $9d$ ,  $18f$ ,  $18h$ , according to Wyckoff notation, are available for R and M atoms, respectively. In the hexagonal phase space group  $P6_3/mmm$  four sites ( $4f$ ,  $6g$ ,  $12j$ ,  $12k$ ) are always occupied by M, while two sites  $2b$  and  $2c$  are available for R. Current knowledge indicates that two metal atoms are symmetrically positioned in a dumbbell configuration with respect to the basal plane of the structure containing the R atoms.

In a paper published by our group studying equilibrium solid phases in the Er-Nd-Fe system at 1073 K Fig. 12 ([27]) shows the X-ray diffraction patterns for the five compositions  $\text{Er}_{2-x}\text{Nd}_x\text{Fe}_{17}$  ( $x=0, 0.5, 1, 1.5$ ). For  $x=0$  we noted that the compound crystallizes in a hexagonal lattice in the space group  $P6_3/mmm$ . The same observation for both compositions  $x=0.5$  and  $x=1$ . However, for the composition with  $x=1.5$ , we noted the presence of peaks of the  $2/17$  rhombohedral phase and the  $2/17$  hexagonal phase. After a total substitution of the Er atom by the Nd atom, the structure becomes pure rhombohedral. From this observation, we can conclude that the change from a hexagonal structure to a rhombohedral structure is not sudden, but it occurs gradually by substituting erbium by neodymium. The Rietveld refinement confirms that neodymium replaces erbium with a change of crystal structure.

In Fig. 2, we present diffractograms obtained from measurements of four compounds, with two being erbium-rich and the other two neodymium-rich. The diffractograms distinctly reveal that the two erbium-rich compounds exhibit a hexagonal  $\text{Th}_2\text{Ni}_{17}$  structure, whereas the neodymium-rich compounds' diffractograms display a rhombohedral  $\text{Th}_2\text{Zn}_{17}$  structure. Upon closer examination of the diffraction peaks, a noticeable trend emerges: with increasing erbium concentration, the diffraction peaks shift towards wider angles. This phenomenon stems from the reduction in lattice parameters caused by the comparatively smaller size of erbium atoms when contrasted with neodymium atoms. This observation is confirmed by Rietveld refinement, and the obtained lattice parameters for all compositions are listed in Tab. I. We display in Fig. 3 the diffractograms of the  $\text{Er}_{2-x}\text{Nd}_x\text{Fe}_{17}$  compounds along with their Rietveld refinement.

The SEM-EDS analysis, which agrees with the results of X-ray diffraction patterns, shows that all the prepared samples are single-phase. Fig.4 presents the SEM image

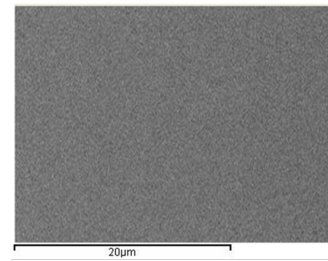


Figure 4. Backscattered electron SEM image of the  $\text{Er}_{1.3}\text{Nd}_{0.7}\text{Fe}_{17}$  compound.

Table II. EDS results of the  $\text{Er}_{2-x}\text{Nd}_x\text{Fe}_{17}$  ( $x = 0, 0.4, 0.7, 1.75, 1.85$  and  $2$ ) compounds.

Compounds	EDS results (at.%)		
	Er	Nd	Fe
$\text{Er}_2\text{Fe}_{17}$	10.43	0	89.57
$\text{Er}_{1.6}\text{Nd}_{0.4}\text{Fe}_{17}$	8.3	2.18	89.52
$\text{Er}_{1.3}\text{Nd}_{0.7}\text{Fe}_{17}$	6.76	3.64	89.5
$0.25\text{Nd}_{1.75}\text{Fe}_{17}$	1.31	9.19	89.32
$\text{Er}_{0.15}\text{Nd}_{1.85}\text{Fe}_{17}$	0.78	9.72	89.41
$\text{Nd}_2\text{Fe}_{17}$	0	10.49	89.51

micrograph of the compound  $\text{Er}_{1.3}\text{Nd}_{0.7}\text{Fe}_{17}$  (as an example). The gray area shows that this sample consists of only one phase without any impurity phase. The details of the compositions measured by EDS are listed as follows in Tab.II

## B. Magnetic and magnetocaloric properties

We present in this part, the magnetic properties of the compounds  $\text{Er}_{2-x}\text{Nd}_x\text{Fe}_{17}$ . In magnetic refrigeration materials, a crucial piece of information is the operating temperature, commonly referred to as the Curie temperature. To estimate the Curie temperature values we measure the magnetization as a function of temperature under a weak external magnetic field Fig. 5(up) shows the variation of the magnetization versus the temperature of the compounds  $\text{Er}_{2-x}\text{Nd}_x\text{Fe}_{17}$  ( $x=0, 0.4, 0.7, 1.75, 1.85, 2$ ).

All the curves exhibit nearly constant magnetization at low temperatures, followed by a sudden drop indicative of the transition from the ferromagnetic state to the paramagnetic state. The transition from the ferromagnetic to the paramagnetic state occurs over a wide temperature range, suggesting that the transition is likely of second order. To determine the Curie temperature, we employ a commonly used method that involves calculating the derivative of magnetization with respect to temperature. According to this method, the Curie temperature corresponds to the minimum of the magnetization derivative.

Fig. 5(down) displays the magnetization derivative

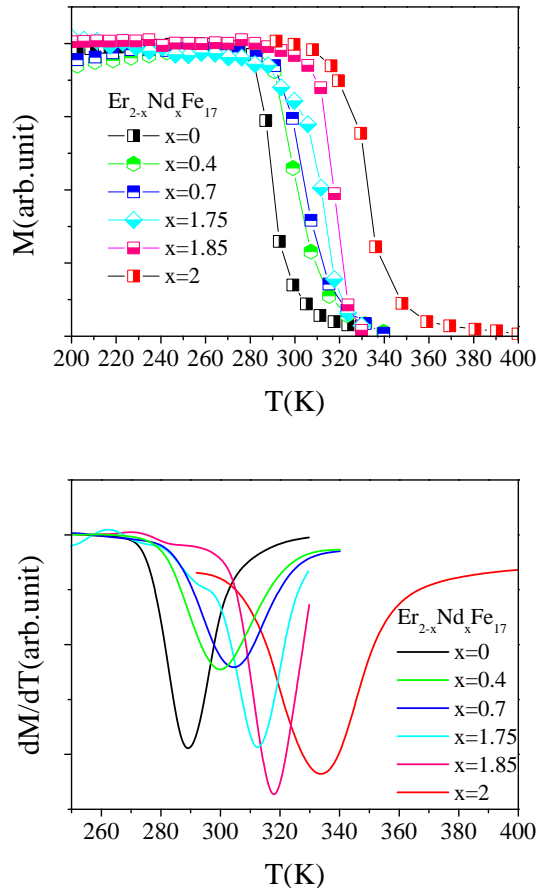


Figure 5. Temperature dependence of magnetization (up) and derivative of magnetization (down) of  $\text{Er}_{2-x}\text{Nd}_x\text{Fe}_{17}$  under an applied magnetic field  $\mu_0 H = 0.1$  T.

curves calculated for the six compositions investigated in this study. We note an increase in the Curie temperature value with the increase of the neodymium compound content. The Curie temperature is equal to 294 K and 335 K for  $\text{Er}_2\text{Fe}_{17}$  and  $\text{Nd}_2\text{Fe}_{17}$ , respectively. This increase is attributed to the de Gennes factor ( $G$ ). The exchange interaction between a rare earth atom and a transition metal is directly proportional to this factor. A higher de Gennes factor leads to a stronger exchange interaction and consequently a higher Curie temperature. Among the rare earth elements, Gd possesses the highest de Gennes factor, which justifies higher Curie temperature of  $\text{Gd}_2\text{Fe}_{17}$  compared to the  $\text{R}_2\text{Fe}_{17}$  series. The factor  $G$  follows an ascending trend from Cerium to Gd and subsequently decreases as one moves away from Gd. Thermomagnetic measurements reveal an initial advantage of these compounds, which is the controllable operating temperature achieved through substitution in the rare earth site.

It's also very important to measure magnetization as a function of the magnetic field in order to compare the saturation magnetization values of the magnetocaloric com-

pounds studied in this article, not only that, but from these curves we can derive other very important information. First, let's look at the saturation magnetization values as a function of neodymium content.

Fig. 6 illustrates the isothermal magnetization behavior, denoted as  $M(\mu_0 H, T)$ , across a range of magnetic fields spanning from 0 to 5 T, while varying temperatures from 252 to 340 K. The data reveals distinct patterns: below the critical temperature  $T_C$ , which signifies the transition to a ferromagnetic state, there is a pronounced upsurge in magnetization with increasing magnetic field strength. Conversely, at temperatures exceeding  $T_C$ , the material exhibits paramagnetic behavior, characterized by a gradual increase in magnetization in response to the applied magnetic field. Additionally, it is noteworthy that, for a constant magnetic field, magnetization diminishes as temperature rises. From Fig. 6, it's clear that magnetization maximum decreases with increasing erbium content. The magnetization maximum values are shown in the Tab. III. In fact, the total moment can be written as  $\mu_{tot} = 17\mu_{Fe} - ((2-x)\mu_{Er} + x\mu_{Nd})$ : in general, in intermetallic compounds that combine a transition metal atom with a rare earth atom, the moments of the rare earth and the moment of the transition metal atom are antiparallel, so the magnetic moment of the rare earth atom is subtracted from the total moment. Since the magnetic moment of erbium is much higher than that of neodymium, compensation is more important, hence the decrease in saturation magnetization.

To determine the variation in magnetic entropy resulting from the application of a magnetic field, we need to perform the following integration using the Maxwell relation [47]:

$$\Delta S_M = \mu_0 \int_0^H \left( \frac{\partial M}{\partial T} \right)_H dH$$

Here,  $M$  represents magnetization,  $T$  represents temperature, and  $\mu_0 H$  represents the applied magnetic field. However, if we obtain isothermal  $M(H)$  curves through discrete changes in the magnetic field, we can utilize the following expression [47]:

$$|\Delta S_M| = \mu_0 \sum_i \frac{M_i - M_{i+1}}{T_{i+1} - T_i} \Delta H_i$$

In this equation,  $M_i$  and  $M_{i+1}$  denote the initial magnetization at temperatures  $T_i$  and  $T_{i+1}$ , respectively, when the magnetic field increases by  $\Delta H_i$ . Table IV presents the values of  $-\Delta S_M$  for various  $\text{R}_2\text{Fe}_{17}$  compounds.

Fig. 7 depicts the magnetic entropy variation in the vicinity of the Curie temperature of  $\text{Er}_{2-x}\text{Nd}_x\text{Fe}_{17}$  compounds with  $x=0.4, 0.7, 1.75$  and  $1.85$  in response to an external magnetic field ranging from 0 to 5 T. At a magnetic field change of  $\mu_0 \Delta H = 5, T$ , the magnitude of  $|\Delta S_M|$  is approximately 6 J/(kg·K) at  $T=320$  K,

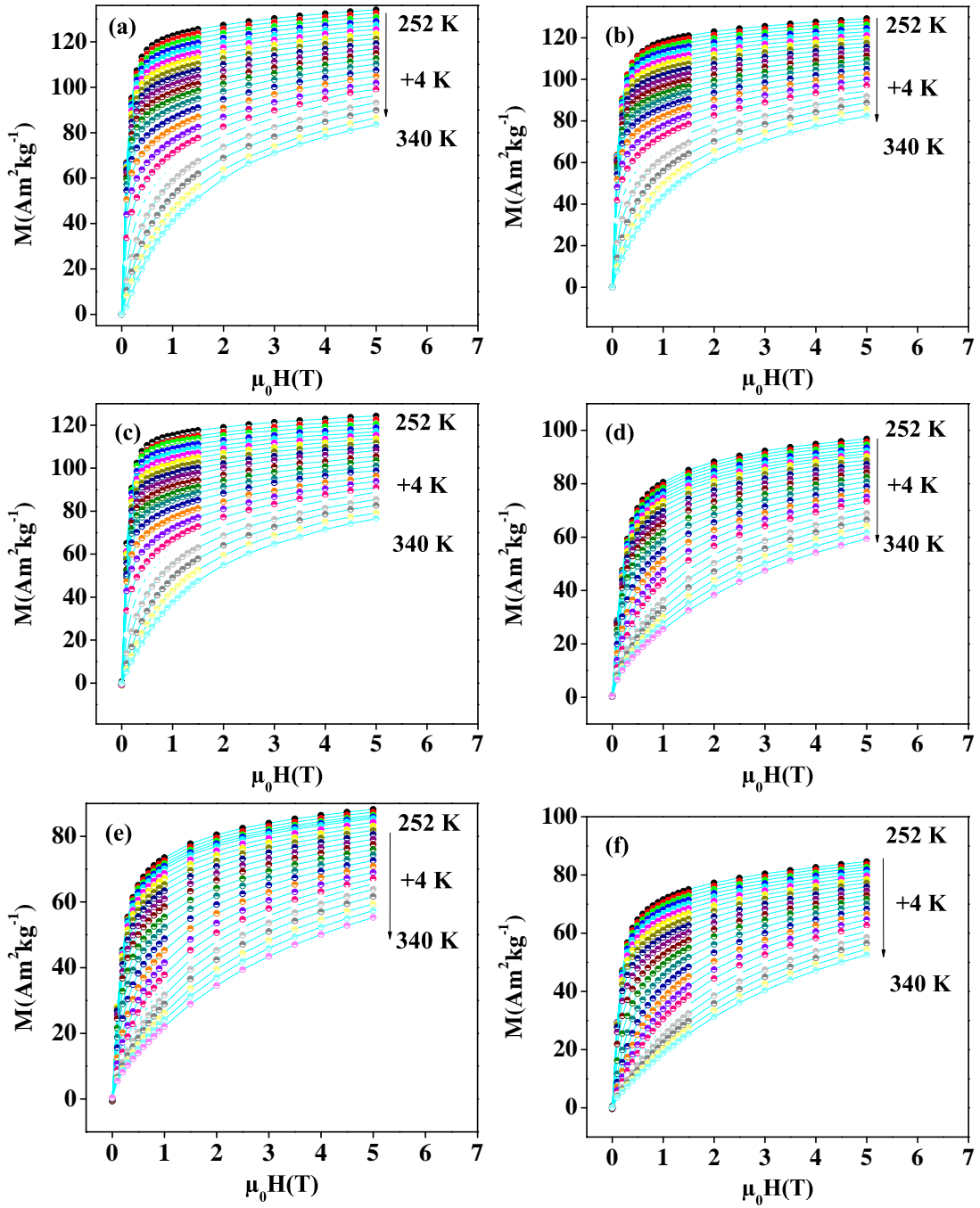


Figure 6. Temperature and magnetic field dependence of magnetization for  $\text{Er}_{2-x}\text{Nd}_x\text{Fe}_{17}$  compounds with  $x=2$  (a),  $x=1.85$  (b),  $x=1.75$  (c),  $x=0.7$  (d),  $x=0.4$  (e) and  $x=0$  (f).

Table III. Magnetization maximum of  $\text{Er}_{2-x}\text{Nd}_x\text{Fe}_{17}$  compounds measured at 252 K under a maximum of an applied magnetic field equal to 5 T.

	$x = 0$	$x = 0.4$	$x = 0.7$	$x = 1.75$	$x = 1.85$	2
$M_{max}$ ( $\text{Am}^2 \cdot \text{kg}^{-1}$ , $T=252$ K)	85	90	97	124	129	135

$T=329$  K and  $T=335$  K for  $x=1.75$ ,  $x=1.85$  and 2, respectively. For  $x=0$ ,  $x=0.4$  and 0.7 the magnitude of  $|\Delta SM|$

is approximately  $3.5$  J/(kg·K) at  $T=295$  K,  $T=308$  K and  $T=315$  K, respectively. The introduction of Nd through

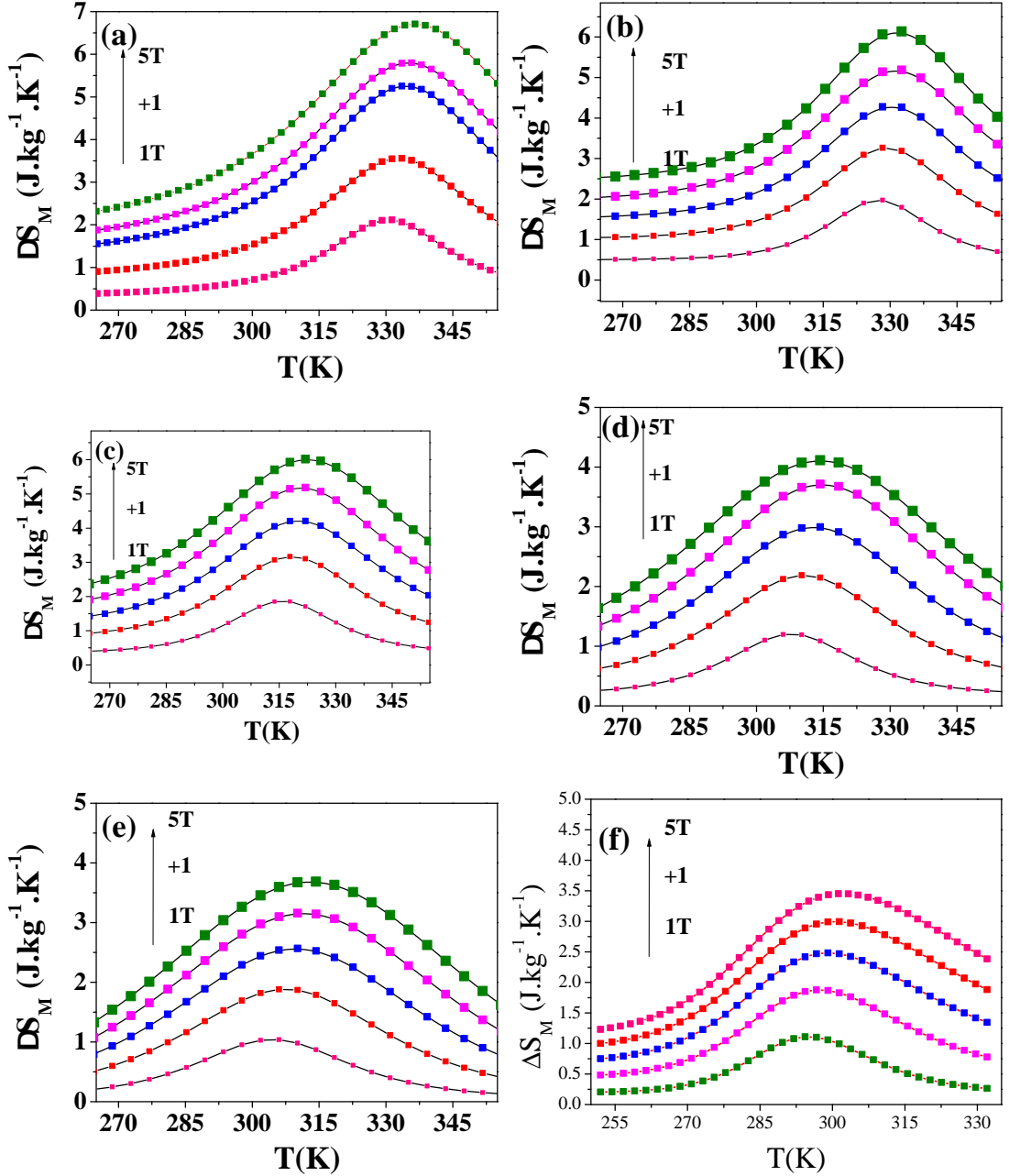


Figure 7. Magnetic entropy change plotted against temperature under several applied magnetic fields for  $\text{Er}_{2-x}\text{Nd}_x\text{Fe}_{17}$  compounds with  $x=2$  (a),  $x=1.85$  (b),  $x=1.75$  (c),  $x=0.7$  (d),  $x=0.4$  (e) and  $x=0$  (f).

partial substitution for Er results in an elevated operational temperature where the maximum of  $|\Delta S_M|$  occurs. All compositions present a good magnetocaloric effect, with a quasi-constant magnetic entropy change. According to the Tab. IV, the maximum variation in magnetic entropy decreases as the erbium concentration increases,  $\Delta S_{max}$  of  $\text{Nd}_2\text{Fe}_{17}$  seeks a maximum for  $T = T_C$  equal to  $6.3 \text{ J}/(\text{kg}\cdot\text{K})$  for a magnetic field variation equal to  $5 \text{ T}$ , whereas for the  $\text{Er}_2\text{Fe}_{17}$  compound the maximum magnetic entropy takes the value  $3.5 \text{ J}/(\text{kg}\cdot\text{K}) \sim 60\%$  of that observed for the  $\text{Nd}_2\text{Fe}_{17}$  compound.

While numerous research studies have reported materials with high Entropy Change effects at low and high temperatures, there are relatively few materials exhibiting high Magnetocaloric Effect (*MCE*) and a second-order transition from a ferromagnetic state to a paramagnetic state around  $300 \text{ K}$ .

The relative cooling power (*RCP*) is a crucial parameter in magnetocaloric applications and is linked to the maximum entropy change as expressed in the following relationship [6]:

$$RCP = -\Delta S_M \delta T^{\text{FWHM}}$$

Table IV.  $T_C$ , magnetic entropy change and magnetic field change of some  $R_2\text{Fe}_{17}$  compounds.

Compound	$T_C$ (K)	$-\Delta S_M$ J/(kg·K)	$\mu_0\Delta H$ (T)	$\delta T^{FWHM}$ (K)	$RC^{area}$ (J/kg)	$RCP$ (J/kg)	Ref
$\text{Er}_2\text{Fe}_{17}$	290	3.5	5	67	275	234.5	This work
$\text{Er}_{1.6}\text{Nd}_{0.4}\text{Fe}_{17}$	300	3.7	5	88.6	258	328	This work
$\text{Er}_{1.3}\text{Nd}_{0.7}\text{Fe}_{17}$	308	4.1	5	100	332	410	This work
$\text{Er}_{0.25}\text{Nd}_{1.75}\text{Fe}_{17}$	315	5.7	5	76	331	433	This work
$\text{Er}_{0.15}\text{Nd}_{1.85}\text{Fe}_{17}$	320	6.1	5	66	302.3	402	This work
$\text{Nd}_2\text{Fe}_{17}$	337	6.3	5	62	280	390	this work
$\text{Y}_2\text{Fe}_{17}$	303	4.6	5	103	367	478	[48]
$\text{Pr}_{1.64}\text{Sm}_{0.36}\text{Fe}_{17}$	300	3.24	3	78	195	247	[49]
Gd	293	4.8	2	44	-	213	[50]
$\text{Pr}_2\text{Fe}_{17}$	285	5.5	5	98	-	540	[51]
$\text{Gd}_2\text{Fe}_{17}$	475	1.2	1.5	-	-	18	[52]
$\text{Nd}_2\text{Fe}_{17}$	339	1.7	1.5	50	-	105	[53]

Compound	$T_{mid}$ K	$\Delta\mu_0H$ T	$\Delta T_{H-C}$ K	$TEC$ $J(K \cdot kg)^{-1}$	$\frac{TEC}{\Delta\mu_0H}$ $J(K \cdot kgT)^{-1}$	Ref
$\text{Er}_2\text{Fe}_{17}$	290	5	5	3.4	0.7	This work
$\text{Er}_{1.6}\text{Nd}_{0.4}\text{Fe}_{17}$	300	5	5	3.8	0.85	This work
$\text{Er}_{1.3}\text{Nd}_{0.7}\text{Fe}_{17}$	308	5	5	4.3	0.98	This work
$\text{Er}_{0.25}\text{Nd}_{1.75}\text{Fe}_{17}$	315	5	5	5.5	1.17	This work
$\text{Er}_{0.15}\text{Nd}_{1.85}\text{Fe}_{17}$	320	5	5	6	1.26	This work
$\text{Nd}_2\text{Fe}_{17}$	330	5	5	6.4	1.32	This work
$\text{Pr}_{1.64}\text{Sm}_{0.36}\text{Fe}_{17}$	300	3	5	3.71	1.24	[49]
$\text{Pr}_{0.5}\text{Eu}_{0.1}\text{Sr}_{0.4}\text{MnO}_3$	279.9	5	5	4.45	0.89	[54]
$\text{Pr}_{0.5}\text{Er}_{0.1}\text{Sr}_{0.4}\text{MnO}_3$	188.5	5	5	4.9	0.98	[54]
$\text{TmFe}_{0.7}\text{Mn}_{0.3}\text{O}_3$	11	7	5	7	1	[55]
$\text{TmFe}_{0.8}\text{Mn}_{0.2}\text{O}_3$	12	7	5	6.4	0.914	[55]
$\text{La}_{0.8}\text{Na}_{0.2}\text{MnO}_3$	330	5	5	4.6	0.92	[56]
$\text{La}_{0.8}\text{Ca}_{0.05}\text{Na}_{0.15}\text{MnO}_3$	315	5	5	4.55	0.91	[56]
$\text{Ho}_2\text{CoMnO}_6$	77	7	5	6.5	0.928	[57]

The parameter  $\delta T^{FWHM}$  represents the full width at half-maximum in the temperature dependence of the magnetic entropy change. Table IV provides the maximum values for  $-\Delta S_M$ , the temperature variation  $\Delta T$ , and the relative cooling power ( $RCP$ ).

Another crucial parameter for assessing the magnetocaloric effect is the refrigerant capacity ( $RC$ )Area, which quantifies the amount of heat that can be transferred during a single thermodynamic cycle. The  $RC$  value is determined by calculating the area under the  $-\Delta S_M$  curve at the temperature corresponding to the FWHM. This can be computed by integrating the following expression [58]:

$$RC_{Area}(H) = \int_{T_{min}}^{T_{max}} \Delta S_M(T, H) dT;$$

$$T_{max} - T_{min} = \delta T^{FWHM}$$

Apart from  $RCP$  and  $RC_{area}$ , there is another parameter known as the temperature-averaged entropy change ( $TEC$ ), which has been employed to assess the suitability of materials for magnetic refrigeration technologies. The concept of  $TEC$  was introduced by L. D. Griffith and his colleagues as an additional figure of merit. The calculation of  $TEC$  involves utilizing magnetic entropy change data and can be expressed as follows [59]:

$$TEC = \frac{1}{\Delta T_{H-C}} \max \left\{ \int_{T_{mid} - \frac{\Delta T_{H-C}}{2}}^{T_{mid} + \frac{\Delta T_{H-C}}{2}} |\Delta S_M(T)| dT \right\}$$

Let  $\Delta T_{H-C}$  denote the temperature range of the measuring device, representing the difference between the hot and cold heat exchangers.  $T_{mid}$  signifies the temperature value at the midpoint of  $\Delta T_{H-C}$ , optimizing ( $TEC$ ) value. Figure 8 illustrates  $TEC$  variation with

$\Delta T_{H-C}$  for magnetic field changes equal to 5 T. Notably,  $TEC$  exhibits a gradual, monotonic decrease as  $\Delta T_{H-C}$  increases, closely approaching the maximum entropy change value for lower  $\Delta T_{H-C}$ . For a given temperature,  $TEC$  consistently increases with the Nd content. Let's now discuss the different figures of merit of the

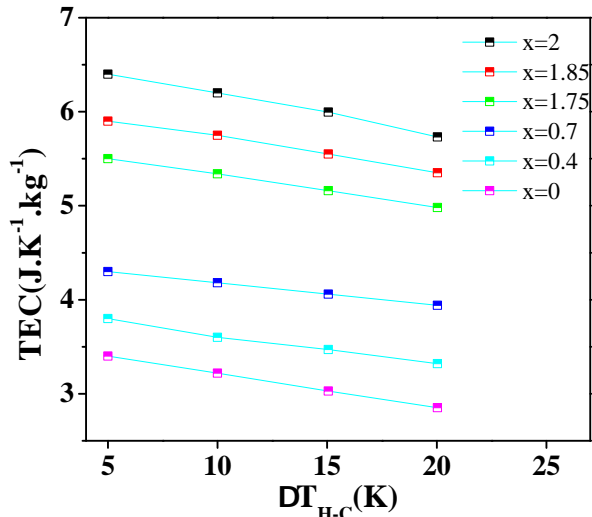


Figure 8.  $TEC$  plotted against  $\Delta T_{H-C}$  for  $Er_{2-x}Nd_xFe_{17}$

magnetocaloric effect calculated in this article. the  $RCP$  calculated for the  $Er_2Fe_{17}$  compound for a magnetic field variation equal to 5 T is equal to 234 J/kg, by increasing the Nd concentration the  $RCP$  value increases to a maximum value equal to 433 J/kg for the  $Er_{0.4}Nd_{1.6}Fe_{17}$  compound, then decreases slightly to reach a value equal to 390 J/kg for the  $Nd_2Fe_{17}$  compound. this anomaly can be explained by the decrease in the width at half the maximum of the magnetic entropy with the increase in Nd concentration, which was not sufficiently compensated by the increase in the maximum of the magnetic entropy to give a monotonic variation of the  $RCP$ , the same behavior is observed in the values of  $RC^{area}$ . There are several magnetocaloric materials that have been studied for magnetic refrigeration at room temperature:  $Gd_5(Ge,Si)_4$  [1–4],  $La(Fe,Co,Si)_{13}(H,C)$  [5–10],  $Fe_2P$  [11–14], manganites  $R_{1-x}A_xMnO_3$  [15–18] and related alloys and compounds. In these materials the magnetic transition from the ferromagnetic state to the paramagnetic state is a first-order transition phase that shows a large  $|\Delta S_M|$  at operating temperature, but possess a low  $RCP$  because of their low working temperature range  $\delta T^{FWHM} \sim 10$  K as opposed to materials with second-order transition phase like the compound  $Er_{1.3}Nd_{0.7}Fe_{17}$  with  $\delta T^{FWHM} \sim 100$  K. For  $Er_{1.3}Nd_{0.7}Fe_{17}$  and  $Er_{0.25}Nd_{1.75}Fe_{17}$   $RCP$  is found to be around 430 J/kg under a magnetic field change of 5 T which is around 70% of that observed in pure Gd and makes our compound a potential candidate for magnetic refrigeration around the room temperature [50].

From the point of view of magnetic refrigeration the irreversibility of the magnetocaloric effect is a major dis-

advantage, indeed, a very small thermal hysteresis is a basic constraint for a practical refrigerant [60]. For example, the materials mentioned above like  $(Gd_5(Ge,Si)_4, La(Fe,Co,Si)_{13}(H,C), Fe_2P)$  exhibit a first-order transition phase, show a large  $|\Delta S_M|$  but with a relatively large thermal hysteresis contrary to materials that display a second-order magnetic transition. Compared to these materials,  $Er_{2-x}Nd_xFe_{17}$  exhibits a second order magnetic transition at a  $T_C$  very close to room temperature with a moderate  $|\Delta S_M|$  and high  $RCP$ .

It should be mentioned that detailed research shows that the Maxwell relation can not be utilized close to the Curie temperature because of the coexistence of paramagnetic and ferromagnetic phases the sudden drop in the magnetization causes a discontinuity in the entropy change at Curie temperature. Consequently, the large entropy peak is a fallacious result because of the inappropriate use of the Maxwell relation [61, 62]. The  $TEC$  values obtained for  $(Er,Nd)_2Fe_{17}$  are shown in tab IV. the  $TEC$  calculated for the  $Er_2Fe_{17}$  compound for a magnetic field variation equal to 5 T is equal to 3.4 J/(kg.k), by increasing the Nd concentration the  $TEC$  value increases to a maximum value equal to 6.4 J/(kg.K) for the  $Nd_2Fe_{17}$  compound. For the variation in the value of  $TEC$ , we observe a monotone variation, and we don't observe a maximum like the one observed for  $RCP$ . This can be explained by the low value of  $\Delta T_{H-C}=5$  K. In this case, the  $TEC$  values follow the same variation observed for the maximum magnetic entropy. To compare  $TEC$  value of our compound with others, we divide  $TEC$  value by the applied magnetic field value. The compounds studied in this work not only exhibit an adjustable operating temperature in the vicinity of room temperature but also demonstrate a comparable to superior ( $TEC$ ) when compared to the compounds presented in the comparison table. The highest  $TEC$  values are observed for the compounds  $Nd_2Fe_{17}$  and  $Er_{0.15}Nd_{1.85}Fe_{17}$ .

#### IV. CONCLUSION

The structural, magnetic, and magnetocaloric properties were investigated for the compounds ( $x=0, 0.4, 0.7, 1.75, 1.85,$  and  $x=2$ ). For the compounds with  $x=0, 0.4,$  and  $0.7$ , they crystallize in a hexagonal lattice of the  $Th_2Ni_{17}$  type in the space group  $P6_3/mmm$ . In contrast, the compounds with  $x=1.75, 1.85,$  and  $x=2$  crystallize in a rhombohedral lattice of the  $Th_2Zn_{17}$  type in the space group  $R\bar{3}m$ . The evolution of the Curie temperature is studied using thermomagnetic measurements under a low applied magnetic field of 0.1 T. It was observed that the Curie temperature increases with the concentration of Nd. Consequently, we report the evolution of saturation magnetization, which also increases with the Nd concentration. The variation of magnetic entropy is calculated for the different compounds. The absolute value of the magnetic entropy change,  $|\Delta S_M|$ , is approximately 6 J/(kg.K) at temperatures of 320 K, 329 K, and 335 K

for values of  $x$  equal to 1.75, 1.85, and 2, respectively. Conversely, for  $x$  values of 0, 0.4, and 0.7, the magnitude of  $|\Delta S_M|$  is approximately 3.5 J/(kg·K) at temperatures of 295 K, 308 K, and 315 K, respectively. The incorporation of Nd through partial substitution for Er leads to an increased operational temperature, where the maximum of  $|\Delta S_M|$  is observed. For  $\text{Er}_{1.3}\text{Nd}_{0.7}\text{Fe}_{17}$  and  $\text{Er}_{0.25}\text{Nd}_{1.75}\text{Fe}_{17}$   $RCP$  is found to be around 430 J/kg under a magnetic field change of 5 T which is around 70% of that observed in pure Gd. The merit figures  $RC_{area}$  and  $TEC$  have also been calculated to evaluate the magnetocaloric effect. The compounds  $\text{Nd}_2\text{Fe}_{17}$  and  $\text{Er}_{0.15}\text{Nd}_{1.85}\text{Fe}_{17}$  exhibit the highest ( $TEC$ ) values

$\sim 1.3 \text{ J}/(\text{Kg}\cdot\text{K})$ . The  $\text{Er}_{2-x}\text{Nd}_x\text{Fe}_{17}$  series offers the advantage of a tunable operating temperature around room temperature with an interesting magnetocaloric effect.

## ACKNOWLEDGMENTS

This work was supported by the National Center for Scientific Research (CNRS), France and the Ministry of Higher Education and Scientific Research MESLab (LR05ES12)

- 
- [1] V. K. Pecharsky and K. A. Gschneidner. *Phys. Rev. Lett.*, 78:4494, 1997.
- [2] V. K. Pecharsky and K. A. Gschneidner. *J. Magn. Magn. Mater.*, 167:L179, 1997.
- [3] K. A. Gschneidner, V. K. Pecharsky, E. Brück, H. G. M. Duijin, and E. M. Levin. *Phys. Rev. Lett.*, 85:4190, 2000.
- [4] H. Tang, V. K. Pecharsky, G. D. Samolyuk, M. Zou, K. A. Gschneidner, V. P. Antropov, D. L. Schlagel, and T. A. Lograsso. *Phys. Rev. Lett.*, 93:237203, 2004.
- [5] S. Fujieda, A. Fujita, and K. Fukamichi. *Appl. Phys. Lett.*, 81:811276–8, 2002.
- [6] A. Fujita, S. Fujieda, and K. Fukamichi. *J. Magn. Magn. Mater.*, 310:e1006–e1007, 2007.
- [7] A. Fujita, S. Fujieda, and K. Fukamichi. *J. Magn. Magn. Mater.*, 321:3553–3558, 2009.
- [8] M. Phejar, V. Paul-Boncour, and L. Bessais. *Intermetallics*, 18:2301, 2010.
- [9] A. Boutahar, M. Phejar, V. Paul-Boncour, L. Bessais, and H. Lassri. *J. Supercond. Nov. Magn.*, 27:1795–1800, 2014.
- [10] M. Phejar, V. Paul-Boncour, and L. Bessais. *J. Solid State Chem.*, 223:95–102, 2016.
- [11] O. Tegus, B. Fuquan, W. Dagula, L. Zhang, E. Brück, P. Z. Si, F. R. de Boer, and K. H. J. Buschow. *J. Alloys Compd.*, 396:6–9, 2005.
- [12] A. Bartok, M. Kustov, L. F. Cohen, A. Pasko, K. Zehani, L. Bessais, F. Mazaleyrat, and M. LoBue. *J. Magn. Magn. Mater.*, 400:333–338, 2016.
- [13] A. Bartok, M. Kuepferling, C. Curcio, V. Basso, A. Pasko, K. Zehani, L. Bessais, F. Mazaleyrat, and M. Lobue. *Refrigeration Science and Technology*, pages 119–122. 2016.
- [14] A. Pasko, A. Bartok, K. Zehani, L. Bessais, F. Mazaleyrat, and M. LoBue. *AIP Advances*, 6:056204, 2016.
- [15] A. R. Dinesen, S. Linderoth, and S. Morup. *J. Phys. Condens. Matter*, 17:6257, 2005.
- [16] Z. Wei, A. Chak-Tong, and D. You-Wei. *Chin. Phys. B*, 22:057501, 2013.
- [17] H. Felhi, M. Smari, A. Bojorek, K. Nouri, E. Dhahri, and L. Bessais. *Prog. Nat. Sci.*, 29:198–209, 2019.
- [18] N. Ameur, F. Elleuch, M. Triki, E. Dhahri, L. Bessais, and E. K. Hlil. *Solid State Comm.*, 289:30–37, 2019.
- [19] K Mandal, A Yan, P Kersch, A Handstein, O Gutfleisch, and KH Müller. *Journal of Physics D: Applied Physics*, 37(19):2628, 2004.
- [20] Haiying Chen, Yan Zhang, Jingzhi Han, Honglin Du, Changsheng Wang, and Yingchang Yang. *J. Magn. Magn. Mater.*, 320(7):1382–1384, 2008.
- [21] P. Alvarez, P. Gorria, J. Sanchez-Llamazares, M. J. Perez, V. Franco, M. Reiffers, I. Curlik, E. Gazo, J. Kovac, and J. A. Blanco. *Intermetallics*, 19:982–987, 2011.
- [22] W. Bouzidi, K. Nouri, T. Bartoli, R. Sedek, H. Lassri, J. Moscovici, and L. Bessais. *J. Magn. Magn. Mater.*, 497:166018, 2020.
- [23] H. Jaballah, W. Bouzidi, R. Fersi, N. Mliki, and L. Bessais. *J. Phys. Chem. Solids*, 161:110438, 2022.
- [24] J. Horcheni, K. Nouri, E. Dhahri, and L. Bessais. *Solid State Chem.*, 326:124219, 2023.
- [25] Z. Gao, L. Li, Y. Ge, S. Zhu, Y. Du, B. Chen, and B. Pan. *J. Alloys Compd*, 935:168060, 2023.
- [26] W-L Zuo, A. Murtaza, Y. Ding, L. Liu, M. Fang, X. Ke, and S. Yang. *Materials Letters*, page 134778, 2023.
- [27] M. Saidi, K. Nouri, S. Walha, L. Bessais, and M. Jemmali. *J. Alloys. Compd*, 844:155754, 2020.
- [28] L. Bessais, E. Dorolti, and C. Djega-Mariadassou. *Appl. Phys. Lett.*, 87, 2005.
- [29] N. Hosni, K. Zehani, T. Bartoli, L. Bessais, and H. Maghraoui-Meherzi. *J. Alloys Compd.*, 694:1295–1301, 2017.
- [30] S. Khazzan, N. Mliki, L. Bessais, and C. Djega-Mariadassou. *J. Magn. Magn. Mater.*, 322(2):224–229, 2010.
- [31] R. Bensalem, W. Tebib, S. Alleg, J. J. Sunol, L. Bessais, and J. M. Greneche. *J. Alloys Compd.*, 471:24–27, 2009.
- [32] K. Zehani, R. Bez, A. Boutahar, EK Hlil, H. Lassri, J. Moscovici, N. Mliki, and L. Bessais. *J. Alloys Compd.*, 591:58–64, 2014.
- [33] A. Hamrita, Y. Slimani, M. K. Ben Salem, E. Hannachi, L. Bessais, F. Ben Azzouz, and M. Ben Salem. *Ceram. int.*, 40:1461–1470, 2014.
- [34] H. Rietveld. *Acta Crystallogr.*, 22:151, 1967.
- [35] H. Rietveld. *J. Appl. Crystallogr.*, 2:65, 1969.
- [36] J. Rodriguez-Carvajal. *Physica B*, 192:55, 1993.
- [37] J. Rodriguez-Carvajal, M. T. Fernandez-Diaz, and J. L. Martinez. *J. Phys.*, 81:210, 2000.
- [38] L. Bessais, S. Sab, C. Djega-Mariadassou, NH. Dan, and NX. Phuc. *Phys Rev B*, 70(13):134401, 2004.
- [39] C. Djega-Mariadassou, L. Bessais, A. Nandra, and E. Burzo. *Phys. Rev. B*, 68:24406, 2003.

- [40] L. Bessais, S. Sab, C. Djega-Mariadassou, N. H. Dan, and N. X. Phuc. *Phys. Rev. B*, 70:134401, 2004.
- [41] K. Younsi, V. Russier, and L. Bessais. *J. Appl. Phys.*, 107:083916, 2010.
- [42] R. Fersi, N. Mliki, L. Bessais, R. Guetari, V. Russier, and M. Cabie. *J. Alloys Compd.*, 522:14–18, 2012.
- [43] Qu. Johnson, D. H. Wood, G. S. Smith, and A. E. Ray. *Acta Crystallogr. B Struct. Cryst. Cryst. Chem*, 24(2):274–276, 1968.
- [44] G. Calestani, N. Magnani, A. Paoluzi, L. Pareti, and C. Rizzoli. *Phys. Rev. B*, 68(5):054424, 2003.
- [45] R. Guetari, R. Bez, C. B. Cizmas, N. Mliki, and L. Bessais. *J. Alloys Compd.*, 579:156–159, 2013.
- [46] S. Khazzan, N. Mliki, and L. Bessais. *J. Appl. Phys.*, 105:103904, 2009.
- [47] M. Foldeaki, R. Chahine, and T. K. Bose. *J. Appl. Phys.*, 77:3528, 1995.
- [48] J.L. Sánchez Llamazares, P. Álvarez-Alonso, C.F. Sánchez-Valdés, P.J. Ibarra-Gaytán, J.A. Blanco, and P. Gorria. *Curr. Appl. Phys.*, 16(9):963–968, 2016.
- [49] H. Jaballah, W. Bouzidi, R. Fersi, N. Mliki, and L. Bessais. *J. Phys. Chem*, 161:110438, 2021.
- [50] V. K. Pecharsky and K. A. Gschneidner Jr. *Phys. Rev. Lett.*, 78(23):4494, 1997.
- [51] R. Guetari, R. Bez, A. Belhadj, K. Zehani, A. Bezergheanu, N. Mliki, L. Bessais, and C. B. Cizmas. *J. Alloys Compd.*, 588:64–69, 2014.
- [52] M. Saidi, K. Nouri, S. Walha, E. Dhahri, A. Kabadou, M. Jemmali, and L. Bessais. *J. Electron. Mater.*, 48:2242–2253, 2019.
- [53] P. Alvarez, J. Sánchez-Marcos, J. Sanchez Llamazares, V. Franco, M. Reiffers, J. Blanco, and P. Gorria. *Acta Phys. Pol*, 118(5):867–869, 2010.
- [54] A. Sakka, R. Mnassri, M.M. Nofal, S. Mahjoub, W. Cheikhrouhou Koubaa, N. Chniba Boudjada, M. Oumezzine, and A. Cheikhrouhou. *J. Magn. Magn. Mater.*, 514:167158, 2020.
- [55] L. Su, X.Q. Zhang, Q.Y. Dong, H. T. Yang and S. H. Li, and Z. H. Cheng. *Ceram. Int*, 47(13):18286–18294, 2021.
- [56] S. Choura-Maatar, M.M. Nofal, R. Mnassri, W. Cheikhrouhou Koubaa, N. Chniba Boudjada, and A. Cheikhrouhou. *J. Mater. Sci.: Mater. Electron.*, 31:1634–1645, 2020.
- [57] D. Mazumdar and I. Das. *J. Appl. Phys.*, 129(6):063901, 2021.
- [58] K.A. Gschneidner Jr., V.K. Pecharsky, A.O. Pecharsky, and C.B. Zimm. In *Materials science forum*, volume 315, pages 69–76. Trans Tech Publ, 1999.
- [59] L. D. Griffith, Y. Mudryk, J. Slaughter, and V. K. Pecharsky. *Journal of Applied Physics*, 123(3):034902, 2018.
- [60] R. C. Zhang, M. F. Qian, X. X. Zhang, F. X. Qin, L. S. Wei, D. W. Xing, X. P. Cui, J. F. Sun, L. Geng, and H. X. Peng. *J. Magn. Magn. Mater.*, 428:464–468, 2017.
- [61] G. J. Liu, J. R. Sun, J. Shen, B. Gao, H. W. Zhang, F. X. Hu, and B. G. Shen. *Appl. Phys. Lett.*, 90(3):032507, 2007.
- [62] M. Balli, D. Fruchart, D. Gignoux, and R. Zach. *Appl. Phys. Lett.*, 95(7):072509, 2009.